iScience, Volume *25*

Supplemental information

Molecular characterization of myotonic dystrophy fibroblast cell lines for use in small molecule screening

Jana R. Jenquin, Alana P. O'Brien, Kiril Poukalov, Yidan Lu, Jesus A. Frias, Hannah K. Shorrock, Jared I. Richardson, Hormoz Mazdiyasni, Hongfen Yang, Robert W. Huigens III, David Boykin, Laura P.W. Ranum, John Douglas Cleary, Eric T. Wang, and J. Andrew Berglund

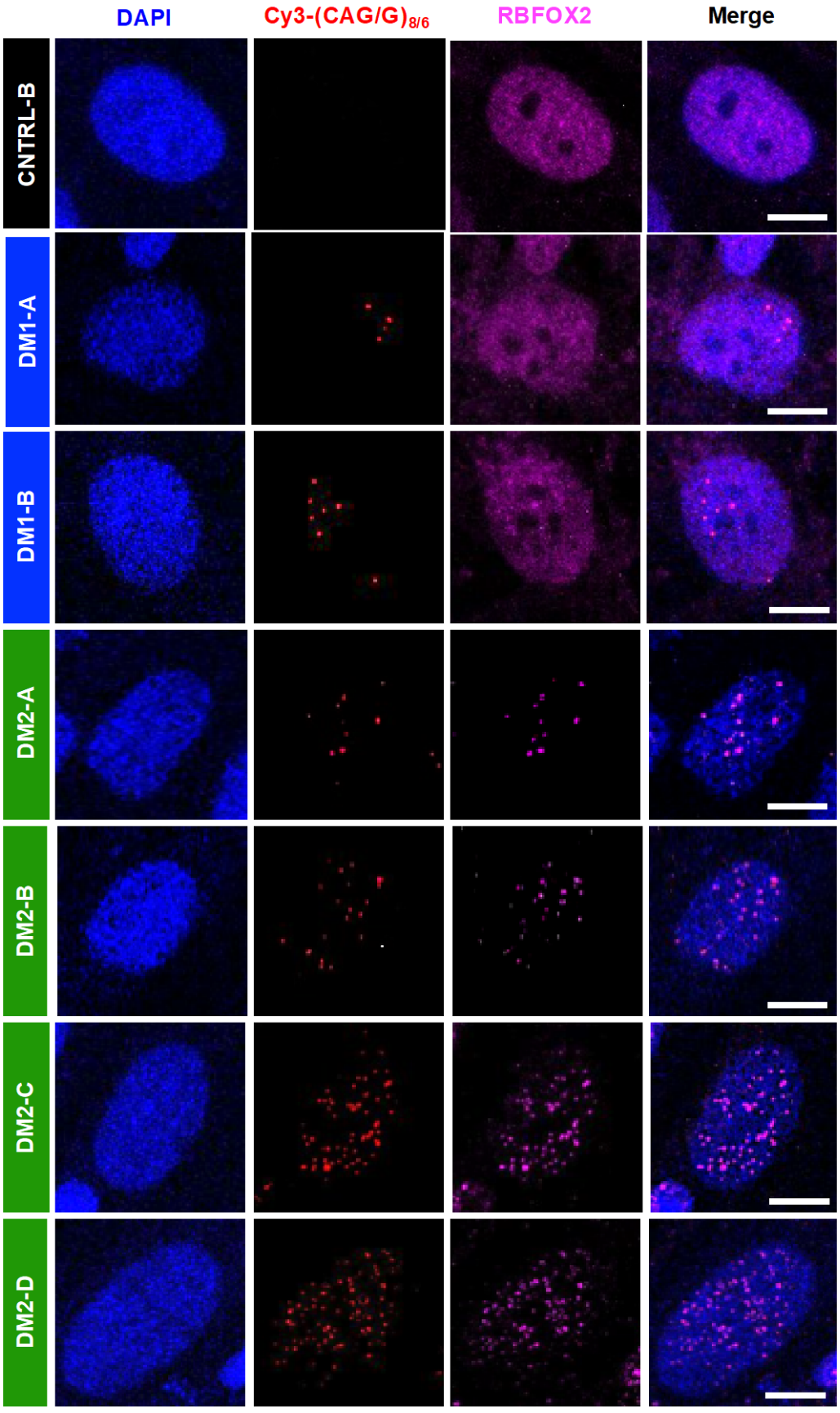
DAPI
Cy3-(CAG/G)8/6
RBFOX2
Merge
CNTRL-B
DM1-A
DM1-B
DM2-A
DM2-B
DM2-C
DM2-D

Figure S1: RBFOX2 immunofluorescence shows co-localization with RNA foci in patient-derived DM2 fibroblasts, related to Figure 1. Fluorescence *in situ* hybridization immunofluorescence (FISH-IF) microscopy in control, DM1 and DM2 fibroblasts against C/CUG RNA using either Cy3-$(CAG)_8$ or -$(CAGG)_6$ probes (red, 2nd column) alongside RBFOX2 immunofluorescence (purple, 3rd column) and DAPI (blue, 1st column). RBFOX2 shows co-localization with CCUG foci in DM2 fibroblasts in contrast to DM1 cells and unaffected cells where RBFOX2 staining is more diffuse in the nucleus. All images were taken using the same laser and contrast/processing settings and a representative scale bar (10μm) is included with each set of micrographs.

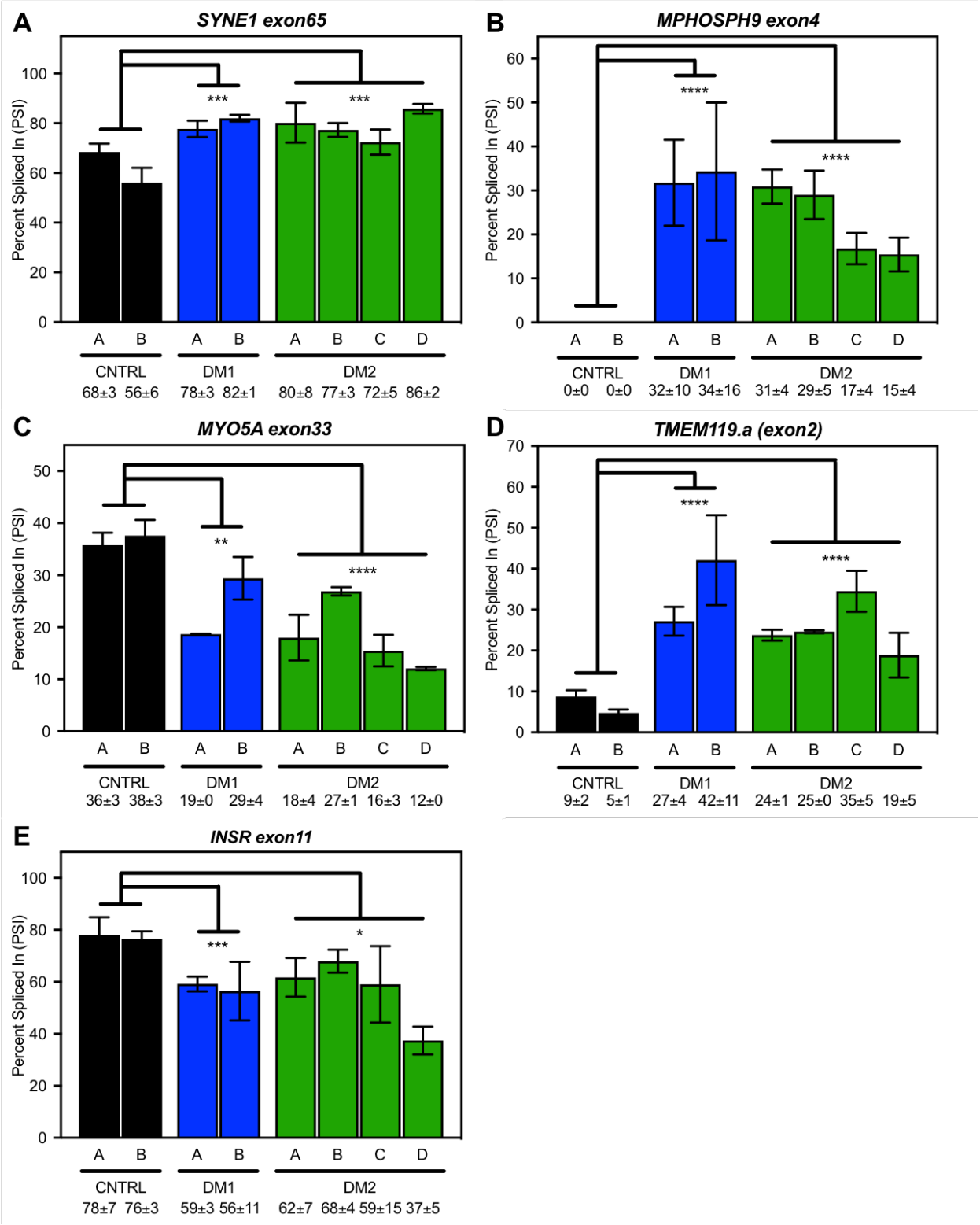

Figure S2: DM1 and DM2 fibroblasts have common mis-spliced alternative exon events confirmed by RNA-seq, related to Figure 2. Splicing analysis of common alternative exon events by RNA-seq for *SYNE1 exon65* (**A**), *MPHOSPH9 exon4* (**B**), *MYO5A exon33* (**C**),

TMEM119.a (exon2) (**D**) and *INSR exon11* (**E**) in control (black), DM1 (blue), and DM2 (green) fibroblasts. The PSI values determined from RNA-seq mirror those observed by RT-PCR analysis (Figure 2). Mean % rescue ± standard deviation values are displayed below each graph (ANOVA two-tailed test, *$p < 0.05$, **$p < 0.01$, ***$p < 0.001$, ****$p < 0.0001$).

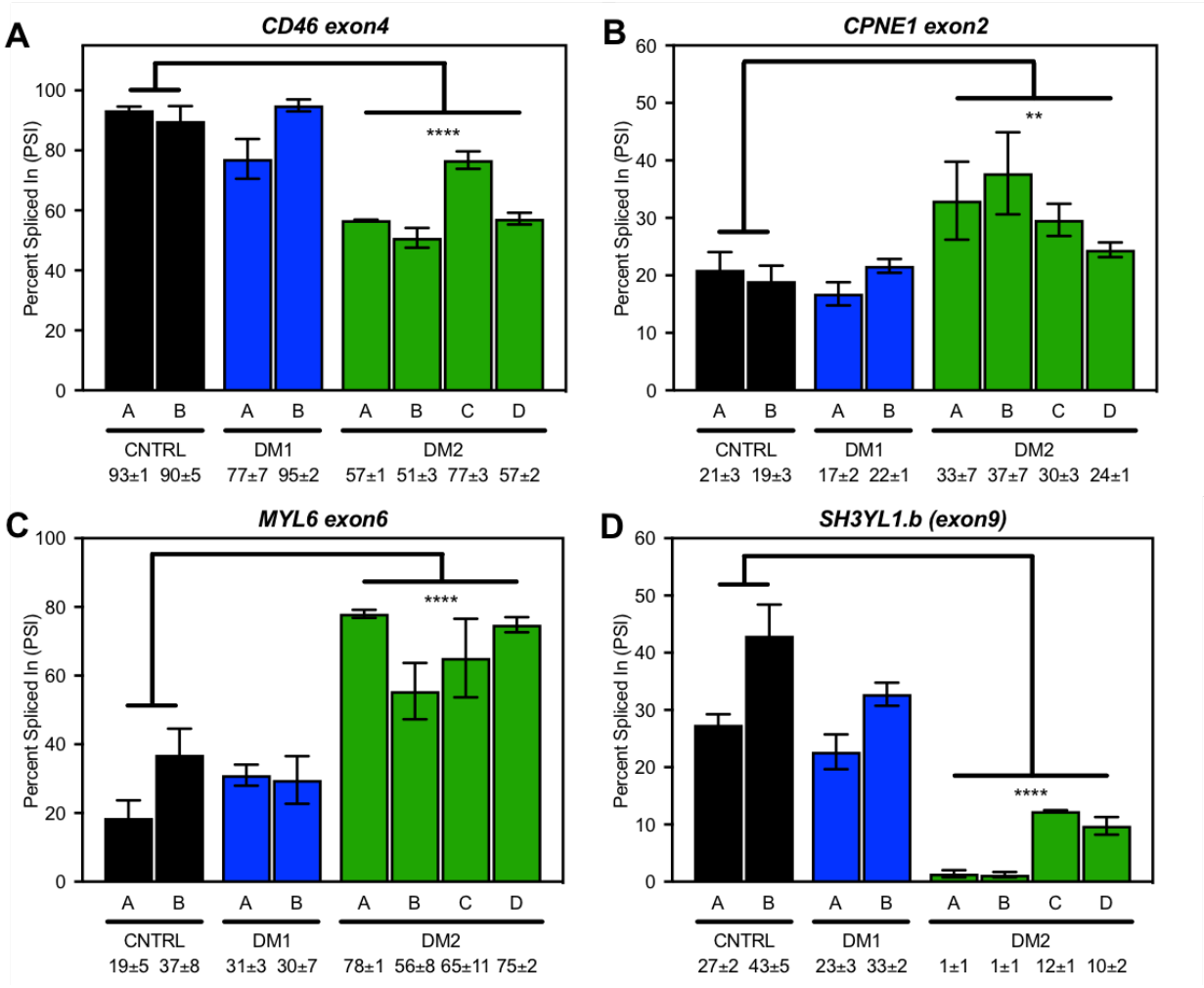

Figure S3: Some alternative exon events are significantly mis-spliced in DM2, but not DM1 fibroblasts, related to Figure 2. RT-PCR splicing analysis of alternative exon events for *CDC46 exon4* (**A**), *CPNE1 exon2* (**B**), *MYL6 exon6* (**C**) and *SYH3YL.b (exon9)* (**D**) in control (black), DM1 (blue), and DM2 (green) fibroblasts. Mean % rescue ± standard deviation values are displayed below each graph (ANOVA two-tailed test, *p < 0.05, **p < 0.01, ***p < 0.001, ****p < 0.0001).

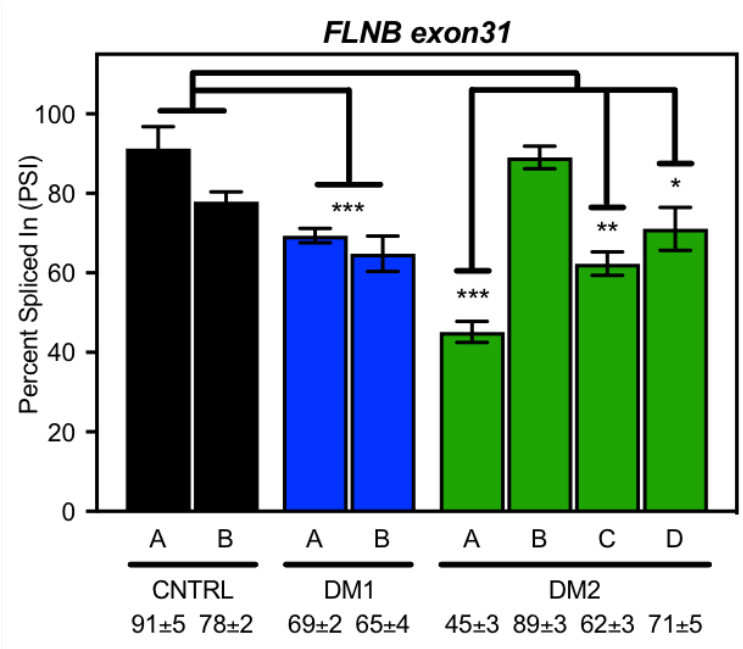

Figure S4: *FLNB exon31* event is mis-spliced in most DM1 and DM2 fibroblasts via RNA-seq, related to Figure 2. Splicing analysis of *FLNB exon31* events via RNA-seq in control (black), DM1 (blue) and DM2 (green) fibroblasts. *FLNB exon31* is mis-spliced in all DM1 and DM2 lines, except DM2-B. Mean % rescue ± standard deviation values are displayed below each graph (ANOVA two-tailed test, *p < 0.05, **p < 0.01, ***p < 0.001).

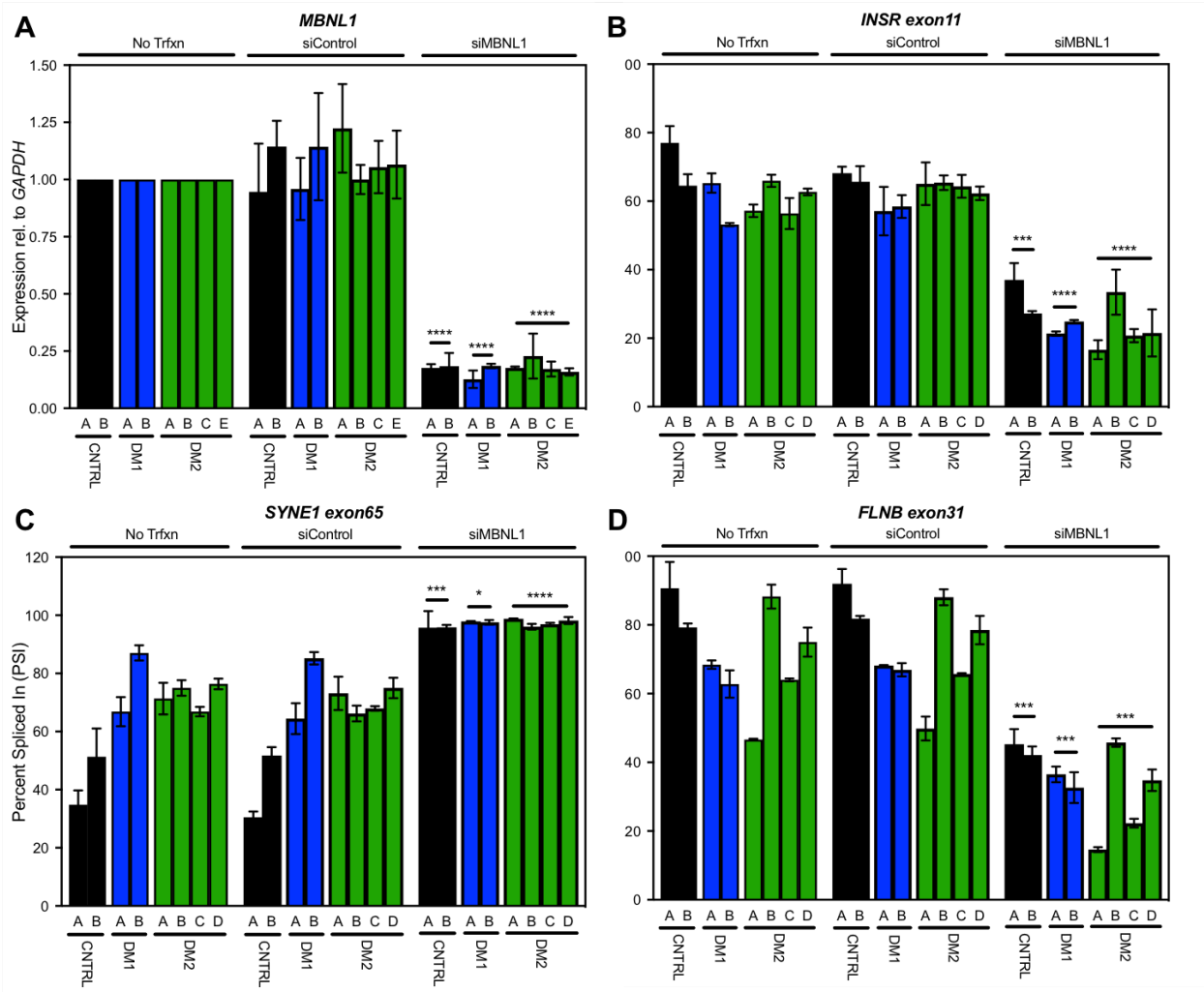

Figure S5: RNAi knockdown of *MBNL1* confirms MBNL1-dependence of common alternative exon events in DM1 and DM2 fibroblasts, related to Figure 2. Expression of *MBNL1* (**A**) and splicing analysis of common AE events (**B-D**) following *MBNL1* knockdown in control (black), DM1 (blue), and DM2 (green) fibroblasts. Fibroblasts were treated with either a control siRNA (siControl) or *MBNL1* siRNA (siMBNL1) for 2 days then *MBNL1* expression via RT-qPCR was determined relative to *GAPDH* (**A).** *MBNL1* expression was calculated relative to expression from non-transfected (No Trfxn) fibroblasts. Splicing analysis by RT-PCR was also examined for the *INSR exon 11* **(B)**, *SYNE1 exon65* **(C)**, and *FLNB exon31* **(D)** events and percent spliced-in (PSI) calculated under each condition following RNAi knockdown. The results confirm the MBNL1-dependence of the *SYNE1* and *FLNB* events, using *INSR exon11* as a positive control. Data are represented as mean % rescue ± standard deviation (ANOVA two-tailed test, *$p < 0.05$, **$p < 0.01$, ***$p < 0.001$, ****$p < 0.0001$).

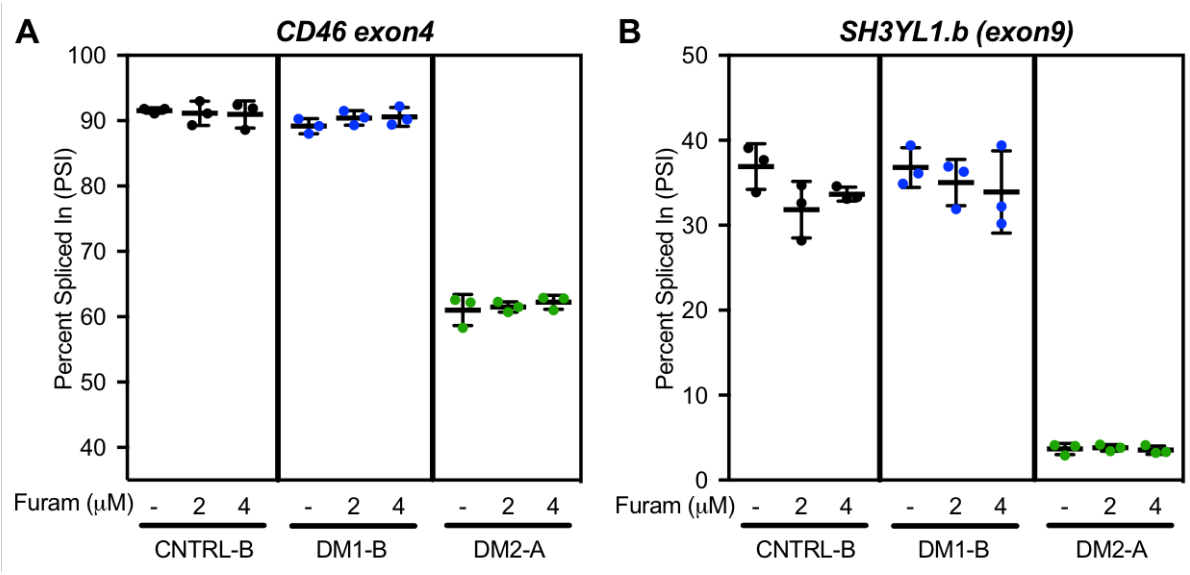

Figure S6: Mis-splicing of DM2-only alternative exon events are not rescued with furamidine treatment in DM2-A line, related to Figure 3. Splicing analysis of *CD46 exon4* **(A)** and *SH3YL1.b (exon9)* **(B)** alternative exon events do not display significant response to furamidine treatment at 2 and 4 μM in CNTRL-B (black), DM1-B (blue), or DM2-A (green) fibroblasts. Data are represented as mean % rescue ± standard deviation.

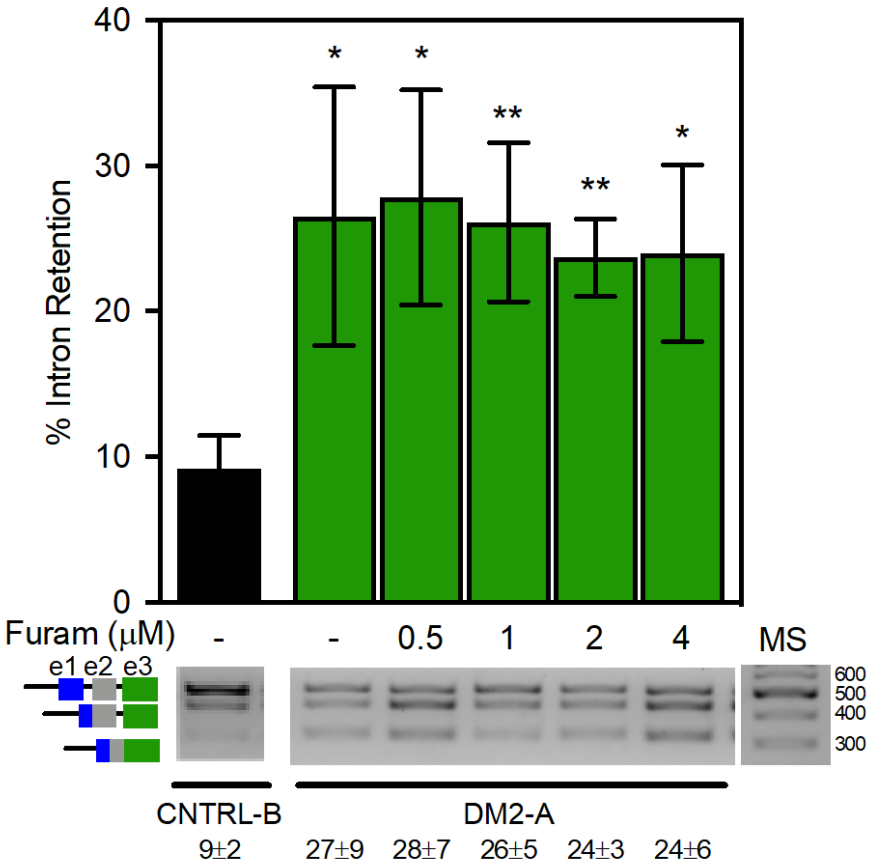

Figure S7: *CNBP intron1* retention is not significantly changed with furamidine treatment in DM2-A line, related to Figure 3. Intron retention assay demonstrated significant *CNBP intron1* retention in DM2-A (green) cell line compared to CNTRL-B line (black). Representative gel image of PCR products using primer set amplifying *intron1* to *exon3* of *CNBP* with product schematic shown left of gel image and mean % intron retention ± standard deviation is denoted below. Molecular standard (MS) values are in base pairs to the right of the gel image. Significance shown is versus CNTRL-B line (ANOVA two-tailed test, *$p < 0.05$, **$p < 0.01$). Data are represented as mean % rescue ± standard deviation. There was no significant change in intron 1 retention with furamidine treatment in the DM2-A versus untreated.

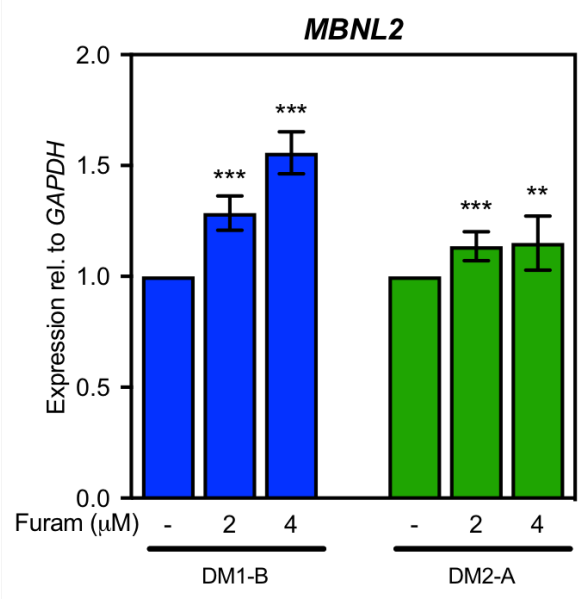

Figure S8: Furamidine increases the expression *MBNL2* transcripts in DM1 and DM2 fibroblasts, related to Figure 3. DM1-B (blue) and DM2-A (green) fibroblast were treated with 2 or 4 μM furamidine for 4 days then assessed for changes in the expression of *MBNL2* transcripts. The expression of *MBNL2* relative to the housekeeping gene *GAPDH* was determined via RT-qPCR and expressed as a percentage relative to untreated fibroblast. Data are represented as mean % rescue ± standard deviation (ANOVA two-tailed test,**$p < 0.01$, ***$p < 0.001$).

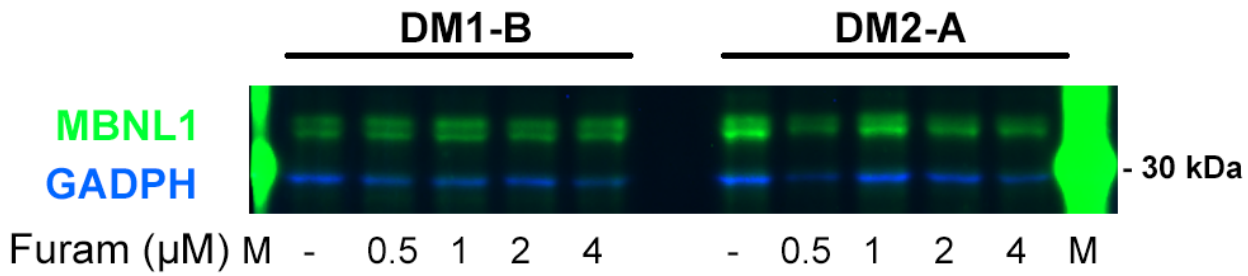

Figure S9: Representative blots for MBNL1 protein in DM1 and DM2 fibroblasts, related to Figure 3. DM1-B and DM2-A fibroblast were treated with 0 (-), 0.5, 1, 2, or 4 μM furamidine for 4 days then assessed for expression of MBNL1 (green) protein via western blot. GAPDH (blue) protein was used as a loading control for reference. Molecular weight markers (M) are show on either side of the sample lanes.

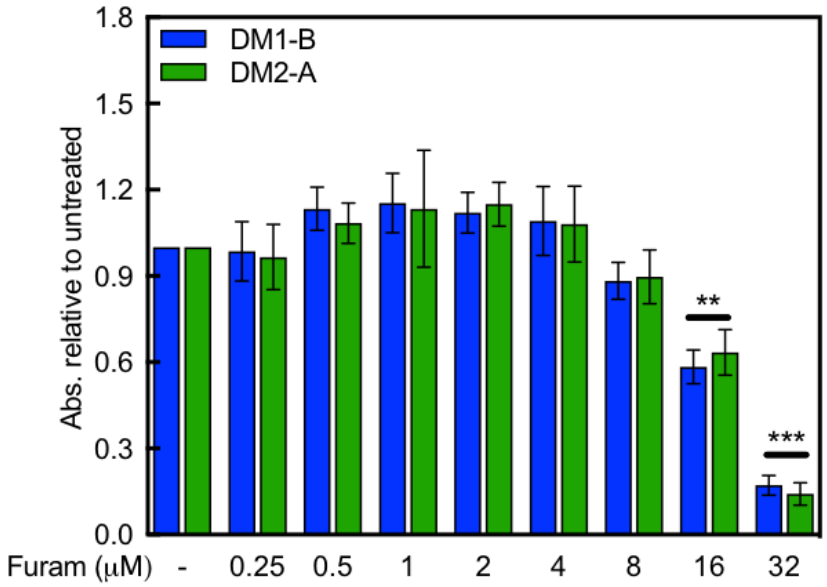

Figure S10: Cell viability of DM1 and DM2 fibroblasts is affected with furamidine treatment at high concentrations, related to Figure 3. DM1-B (blue) and DM2-A (green) fibroblast were treated with a series of concentrations of furamidine (0 to 32 μM) for 4 days then assessed for cell viability via PrestoBlue viability assay (ThermoFisher) using absorbance (560 nm). Furamidine showed significant toxicity after 8 μM. Viability for each concentration was calculated relative to untreated cells. Data are represented as mean % rescue ± standard deviation (ANOVA two-tailed test,**$p < 0.01$, ***$p < 0.001$).

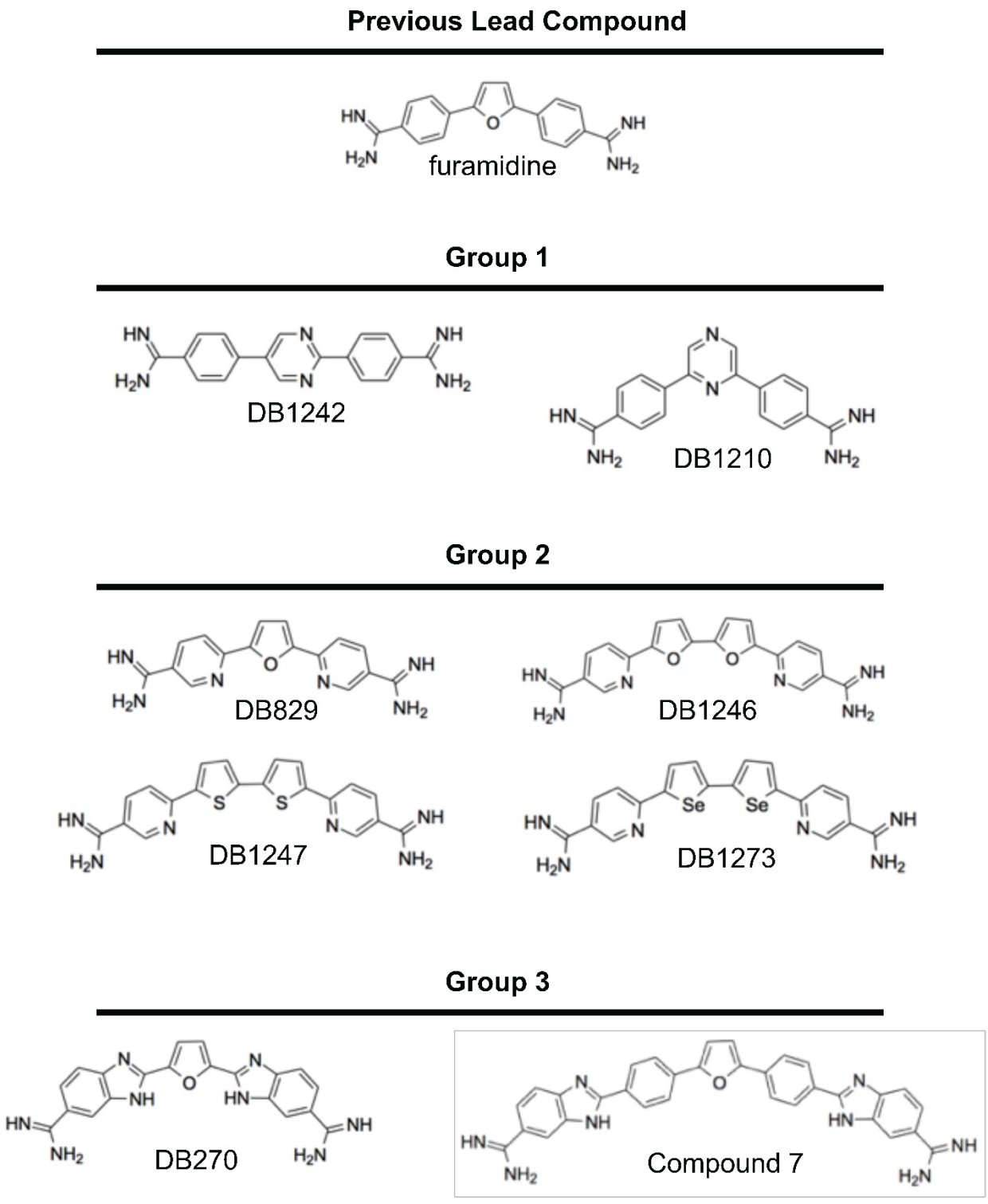

Figure S11: Chemical structures of furamidine and the diamidine analogues used in screen, related to Figure 4. DB1242 and DB1210, the first group of derivatives (**Group 1**), are bis-benzamidines like furamidine (**Previous Lead Compound**), but have central diazine rings as

opposed to a furan linker. DB1242 has a fixed linear shape and has demonstrated higher GC-rich binding affinity over classic AT-rich minor groove binding diamidines like furamidine [1]. DB1210 has a crescent-shape predicted to fit more readily in the DNA minor groove, but retains an analogous hydrogen bonding profile to that of DB1242 [2]. The second group (**Group 2**), DB829, DB1246, DB1247, and DB1273, are aza-analogues of furamidine. DB829 previously showed reduced liver and kidney accumulation and significantly improved brain penetration over furamidine for treatment of stage two human African trypanosomiasis [3, 4]. DB1246, DB1247, and DB1273 are derivatives of DB829, but have double furan, thiophene, and selenophene linkers, respectively. These compounds have previously been shown to bind and stabilize the GGGGCC G-quadruplex repeat RNA associated with *C9orf72* ALS/FTD [5]. The third group (**Group 3**), DB270 and Compound 7, have furan linkers with bis-benzimidazole amidine groups which have been shown to bias binding towards more GC-rich DNA sequences [6]. DB270 has increased cell-permeability and effectiveness as a transcription factor inhibitor [7]. Compound 7 has an extended aromatic system with the substitution of bis-benzimidazole amidines for the amidine groups of furamidine, which can result in higher affinity for DNA sequences due to the ability to span a larger number of bases in the minor groove [8].

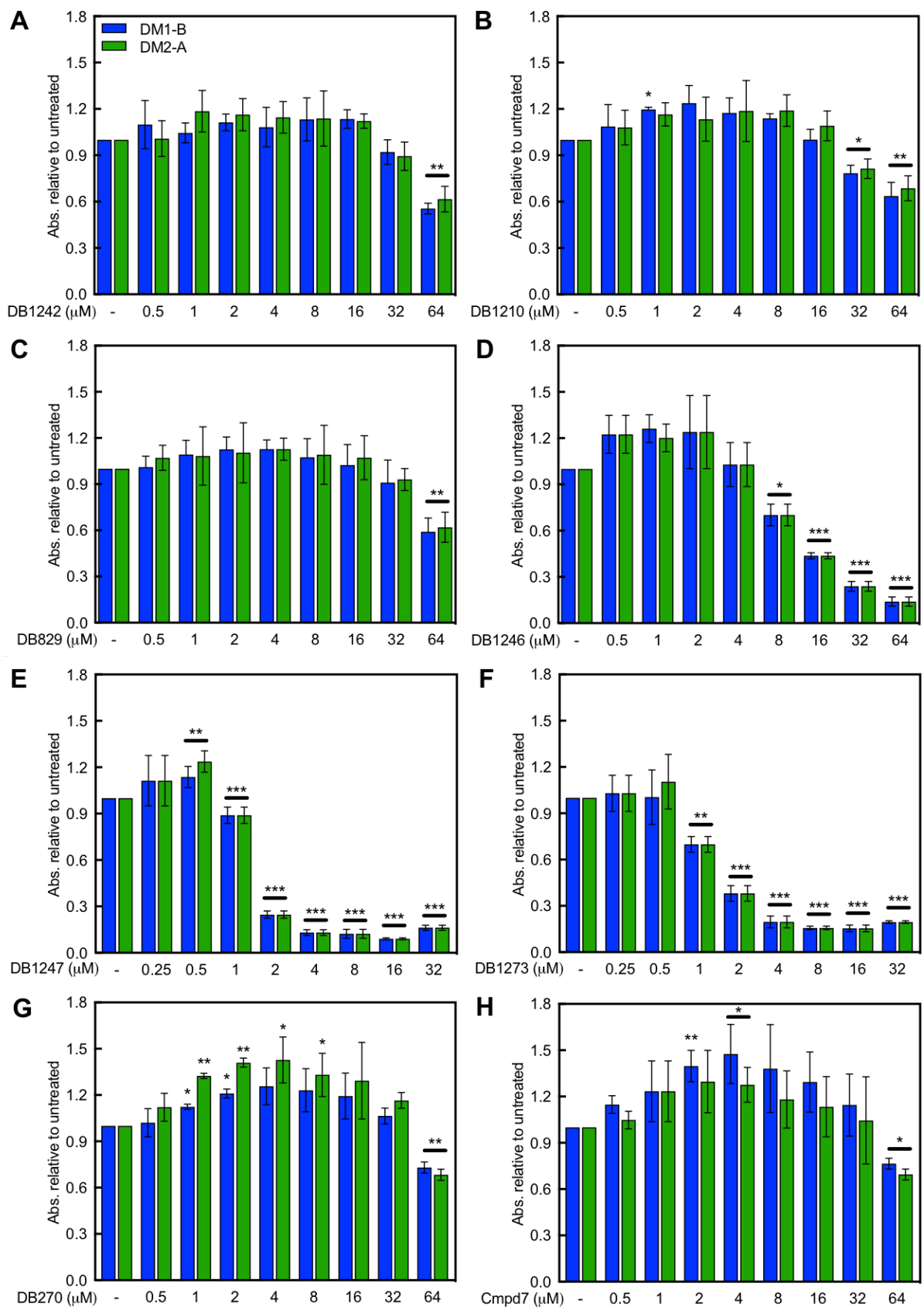
A
DM1-B
DM2-A
Abs. relative to untreated
DB1242 (μM) - 0.5 1 2 4 8 16 32 64
B
DB1210 (μM) - 0.5 1 2 4 8 16 32 64
C
DB829 (μM) - 0.5 1 2 4 8 16 32 64
D
DB1246 (μM) - 0.5 1 2 4 8 16 32 64
E
DB1247 (μM) - 0.25 0.5 1 2 4 8 16 32
F
DB1273 (μM) - 0.25 0.5 1 2 4 8 16 32
G
DB270 (μM) - 0.5 1 2 4 8 16 32 64
H
Cmpd7 (μM) - 0.5 1 2 4 8 16 32 64

Figure S12: Selected diamidines used in screen have variable effects on cell viability of DM1 and DM2 fibroblasts, related to Figure 4. DM1-B (blue) and DM2-A (green) fibroblasts were treated with a series of concentrations of DB1242 **(A)**, DB1210 **(B)**, DB829 **(C)**, DB1246 **(D)**, DB1247 **(E)**, DB1273 **(F)**, DB270 **(G)**, or Cmpd7 **(H)** (0 to 64 μM) for 4 days then assessed for cell viability via PrestoBlue viability assay (ThermoFisher) using absorbance (560 nm). All compounds displayed toxicity at 64 μM. DB1210 started displaying toxicity at 32 μM. Group 2 had compounds with the greatest toxicity with DB1246 displaying toxicity starting at 8 μM, while DB1247 and DB1273 showed significant toxicity after 1 μM and were not tested at concentrations higher than 32 μM. Viability for each concentration was calculated relative to untreated cells. Data are represented as mean % rescue ± standard deviation (ANOVA two-tailed test,*$p < 0.05$, **$p < 0.01$, ***$p < 0.001$).

References

1. Munde M, Ismail MA, Arafa R, Peixoto P, Collar CJ, Liu Y, Hu L, David-Cordonnier MH, Lansiaux A, Bailly C *et al*: **Design of DNA minor groove binding diamidines that recognize GC base pair sequences: a dimeric-hinge interaction motif**. *Journal of the American Chemical Society* 2007, **129**(44):13732-13743.
2. Hu L, Patel A, Bondada L, Yang S, Wang MZ, Munde M, Wilson WD, Wenzler T, Brun R, Boykin DW: **Synthesis and antiprotozoal activity of dicationic 2,6-diphenylpyrazines and aza-analogues**. *Bioorg Med Chem* 2013, **21**(21):6732-6741.
3. Paine MF, Wang MZ, Generaux CN, Boykin DW, Wilson WD, De Koning HP, Olson CA, Pohlig G, Burri C, Brun R *et al*: **Diamidines for human African trypanosomiasis**. *Current opinion in investigational drugs (London, England : 2000)* 2010, **11**(8):876-883.
4. Thuita JK, Wang MZ, Kagira JM, Denton CL, Paine MF, Mdachi RE, Murilla GA, Ching S, Boykin DW, Tidwell RR *et al*: **Pharmacology of DB844, an orally active aza analogue of pafuramidine, in a monkey model of second stage human African trypanosomiasis**. *PLoS neglected tropical diseases* 2012, **6**(7):e1734.
5. Simone R, Balendra R, Moens TG, Preza E, Wilson KM, Heslegrave A, Woodling NS, Niccoli T, Gilbert-Jaramillo J, Abdelkarim S *et al*: **G-quadruplex-binding small molecules ameliorate C9orf72 FTD/ALS pathology in vitro and in vivo**. *EMBO molecular medicine* 2018, **10**(1):22-31.
6. Bailly C, Tardy C, Wang L, Armitage B, Hopkins K, Kumar A, Schuster GB, Boykin DW, Wilson WD: **Recognition of ATGA sequences by the unfused aromatic dication DB293 forming stacked dimers in the DNA minor groove**. *Biochemistry* 2001, **40**(33):9770-9779.
7. Stephens DC, Kim HM, Kumar A, Farahat AA, Boykin DW, Poon GM: **Pharmacologic efficacy of PU.1 inhibition by heterocyclic dications: a mechanistic analysis**. *Nucleic acids research* 2016, **44**(9):4005-4013.
8. Hopkins KT, Wilson WD, Bender BC, McCurdy DR, Hall JE, Tidwell RR, Kumar A, Bajic M, Boykin DW: **Extended aromatic furan amidino derivatives as anti-Pneumocystis carinii agents**. *Journal of medicinal chemistry* 1998, **41**(20):3872-3878.